Brief report Related Commentary, page 4336

Circulating αKlotho influences phosphate handling by controlling FGF23 production

Rosamund C. Smith,[1] Linda M. O'Bryan,[1] Emily G. Farrow,[2] Lelia J. Summers,[2] Erica L. Clinkenbeard,[2] Jessica L. Roberts,[2] Taryn A. Cass,[2] Joy Saha,[1] Carol Broderick,[1] Y. Linda Ma,[1] Qing Qiang Zeng,[1] Alexei Kharitonenkov,[3] Jonathan M. Wilson,[1] Qianxu Guo,[4] Haijun Sun,[4] Matthew R. Allen,[5] David B. Burr,[5] Matthew D. Breyer,[1] and Kenneth E. White[2]

[1]Biotechnology Discovery Research, Lilly Research Laboratories, Eli Lilly and Company, Indianapolis, Indiana, USA. [2]Department of Medical and Molecular Genetics, Indiana University School of Medicine, Indianapolis, Indiana, USA. [3]Diabetes Discovery Research, Lilly Research Laboratories, Eli Lilly and Company, Indianapolis, Indiana, USA. [4]ImClone Systems Inc., New York, New York, USA. [5]Department of Anatomy and Cell Biology, Indiana University School of Medicine, Indianapolis, Indiana, USA.

The FGF23 coreceptor αKlotho (αKL) is expressed as a membrane-bound protein (mKL) that forms heteromeric complexes with FGF receptors (FGFRs) to initiate intracellular signaling. It also circulates as an endoproteolytic cleavage product of mKL (cKL). Previously, a patient with increased plasma cKL as the result of a translocation [t(9;13)] in the α*KLOTHO* (*KL*) gene presented with rickets and a complex endocrine profile, including paradoxically elevated plasma FGF23, despite hypophosphatemia. The goal of this study was to test whether cKL regulates phosphate handling through control of FGF23 expression. To increase cKL levels, mice were treated with an adeno-associated virus producing cKL. The treated groups exhibited dose-dependent hypophosphatemia and hypocalcemia, with markedly elevated FGF23 (38 to 456 fold). The animals also manifested fractures, reduced bone mineral content, expanded growth plates, and severe osteomalacia, with highly increased bone *Fgf23* mRNA (>150 fold). cKL activity in vitro was specific for interactions with FGF23 and was FGFR dependent. These results demonstrate that cKL potently stimulates FGF23 production in vivo, which phenocopies the *KL* translocation patient and metabolic bone syndromes associated with elevated FGF23. These findings have important implications for the regulation of αKL and FGF23 in disorders of phosphate handling and biomineralization.

Introduction

The bone-derived hormone FGF23 and its coreceptor αKlotho (αKL) are critical regulators of systemic phosphate metabolism. The αKL gene product is expressed as multiple species; the membrane-bound form (mKL) associates with FGF23 and FGF receptors (FGFRs) to signal through the MAPK cascade (1, 2). Two soluble species have also been reported, an alternatively spliced secreted form (sKL) (exons 1–3 of the 5-exon *KL* gene) and an endoproteolytic cleavage product of mKL (cKL) (3). Although sKL was identified as a potential αKL variant, only cKL protein was detectable in human and rodent plasma and cerebrospinal fluids (4). The cKL form has been implicated in directly mediating renal phosphate handling through paracrine activity (5); however, whether endocrine effects of cKL occur remains unclear. This possibility is highlighted by findings in a patient with a translocation in the α*KLOTHO* (*KL*) gene (t9;13), who presented with elevated plasma cKL and a ricketic phenotype (6). The biochemical and endocrine abnormalities were complex and included hypophosphatemia, hypocalcemia, inappropriately normal $1,25(OH)_2$ vitamin D (1,25D), and severe hyperparathyroidism requiring surgical intervention. Of note, this patient also had sustained, highly elevated plasma FGF23 (>12 times the upper limit of normal), despite marked hypophosphatemia on or off calcitriol treatment (6). The paradoxically elevated FGF23 in this patient, together with a clinical phenotype resembling that of patients with severe autosomal dominant hypophosphatemic rickets, X-linked hypophosphatemia, and tumor-induced osteomalacia (7), is consistent with cKL functioning to direct the expression of FGF23. The goal of this study was to examine the ability of circulating cKL to act as an endocrine regulator of phosphate metabolism through controlling FGF23 production.

Results and Discussion

Effects of cKL on phosphate metabolism in vivo. To test the role of cKL in phosphate metabolism, mouse cKL was delivered to mice through adeno-associated virus 2/8 (AAV-cKL) under the regulation of a hepatic-specific promoter. Following AAV-cKL treatment, serum phosphate was dose-dependently reduced from 2 weeks through 8 weeks (Figure 1A). The vehicle- and AAV-LacZ–injected mice maintained normal serum phosphate, with no significant differences between these 2 control groups at any time point. Serum calcium was variable between the groups at 2 weeks; however, by 4 to 8 weeks, the AAV-cKL mice were significantly hypocalcemic (Figure 1B). The effects of AAV-cKL expression on endocrine regulators of phosphate and calcium handling were next examined. At weeks 2 through 8, both of the AAV-cKL groups had increased plasma cKL (6 to 13 fold; Figure 1C), consistent with the robust detection of cKL in liver lysates by immunoblot (Figure 1C, inset). Furthermore, compared with controls, serum FGF23 levels were markedly elevated in the AAV-cKL groups (38 to 456 fold; Figure 1D). At week 2 in the high-dose group and in both the low- and high-dose cohorts at week 8, the AAV-cKL–treated mice also exhibited hyperparathyroidism (Figure 1E).

Molecular and skeletal manifestations of cKL expression. Quantitative RT-PCR (qPCR) demonstrated a 150-fold elevation of bone

Conflict of interest: Kenneth E. White receives royalties for licensing the *FGF23* gene to Kyowa Hakko Kirin Co. Ltd.

Citation for this article: *J Clin Invest.* 2012;122(12):4710–4715. doi:10.1172/JCI64986.

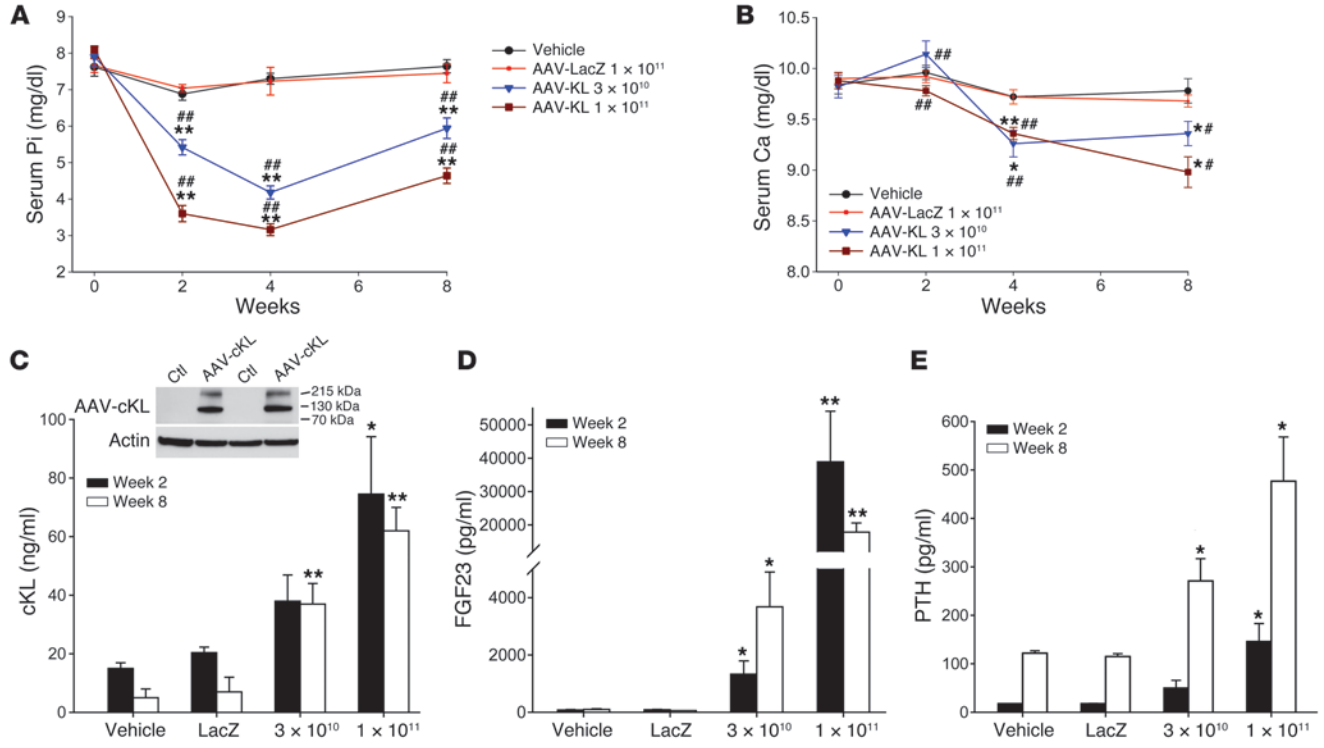

Figure 1

Biochemical and endocrine effects of AAV-cKL in vivo. (**A**) Mice treated with AAV-cKL (3×10^{10} or 1×10^{11} gc per mouse) developed dose-dependent hypophosphatemia by 2 weeks of treatment and (**B**) hypocalcemia by 4 to 8 weeks (n = 5–8 per group; $P < 0.05$ vs. AAV-LacZ or vehicle). $^{*}P \le 0.05$ vs. vehicle; $^{**}P \le 0.001$ vs. vehicle; $^{\#}P \le 0.05$ vs. LacZ; $^{\#\#}P \le 0.001$ vs. LacZ. (**C**) cKL ELISA showed dose-dependent increases in serum cKL at 2 and 8 weeks of AAV-cKL expression, whereas vehicle and AAV-LacZ controls showed no increases above baseline concentrations (n = 5–8 per group; $P < 0.05$ vs. vehicle and AAV-LacZ). In the inset, the immunoblot shows expression of cKL in AAV-cKL mouse liver compared with that of vehicle control (Ctl). β-Actin was used to normalize gel loading. $^{*}P < 0.05$; $^{**}P < 0.001$ vs. vehicle and AAV-LacZ. (**D**) Serum intact FGF23 was markedly elevated in the AAV-cKL groups at 2 and 8 weeks ($^{*}P < 0.01$; $^{**}P < 0.005$). (**E**) PTH was also increased in the AAV-cKL groups ($^{*}P < 0.01$). Values are shown as mean ± SEM.

Fgf23 mRNA in the AAV-cKL–treated mice (Figure 2A). The downstream targets, *Egr1* and *c-fos* mRNAs, both known to be responsive to FGF23-αKL activity (8, 9), were also upregulated in bone (Figure 2B). Kidneys had reduced mRNA expression of the type IIa sodium-phosphate cotransporter (*Npt2a*, also known as *Slc34a1*; Figure 2C) and vitamin D 1α-hydroxylase (*Cyp27b1*; Figure 2D), with elevated vitamin D 24-hydroxylase (*Cyp24*; Figure 2E) mRNA. *KL* mRNA was not different between groups (Figure 2F). These effects are consistent with increased circulating Fgf23 and opposite to findings in animals made hypophosphatemic through low-phosphate diet (10). The skeletal changes in the high-dose AAV-cKL group were dramatic, as micro-CT (μCT) revealed that distal and midshaft femora had significantly reduced bone mineral density (BMD) and bone mineral content (BMC), and lumbar vertebrae had reduced BMC and total area (Table 1). Further, widened growth plates were detected in the distal femora and tibias (Figure 2G). Radiography revealed lower femoral radiodensity and spontaneous fractures (Figure 2H), which were accompanied by severe osteomalacia, as evaluated by histopathology (Figure 2I). Histomorphometry demonstrated that the amount of mineralized trabecular bone was lower in AAV-cKL animals, yet these mice had significant nonmineralized tissue, increasing the total amount of mineralized and nonmineralized tissue volume to 8-fold higher in the AAV-cKL–treated mice compared with that in control mice ($P < 0.01$; Supplemental Table 1; supplemental material available online with this article; doi:10.1172/JCI64986DS1).

Bioactivity of recombinant cKL. Enhanced cell viability through antiapoptotic effects is a known readout for cKL bioactivity (11). NIH3T3 cells were treated with increasing concentrations of cKL and FGF23 either alone or in combination. Following serum withdrawal, the combination of FGF23 plus cKL markedly increased cell viability (EC_{50}, 1 nM; Figure 3A) at concentrations several orders of magnitude less than those required for either FGF23 or cKL alone (EC_{50}, >5 μg/ml; Figure 3A). The effects of cKL were specific to FGF23 since treatment with either FGF19 or 21, endocrine FGFs that interact with the β-Klotho coreceptor, did not prevent cell apoptosis (Figure 3B). A pan-FGFR inhibitor, but not its inactive isomer, dramatically decreased the cell survival effects of cKL and FGF23, supporting that the actions of cKL and FGF23 are FGFR mediated (Figure 3C). Further, following transfection of the FGFR-negative cell line L6 with FGFR1c, FGF23 plus cKL, but not FGF21 plus cKL, stimulated FGFR1 and ERK1/2 phosphorylation (Figure 3D).

These findings show that cKL-dependent stimulation of FGF23 production "overrides" low serum phosphate, a strong physiological suppressor of FGF23, and is consistent with the clinical profile of a described patient with *KL* translocation (6). In this regard, mice exposed to cKL manifested hypophosphatemia (Fig-

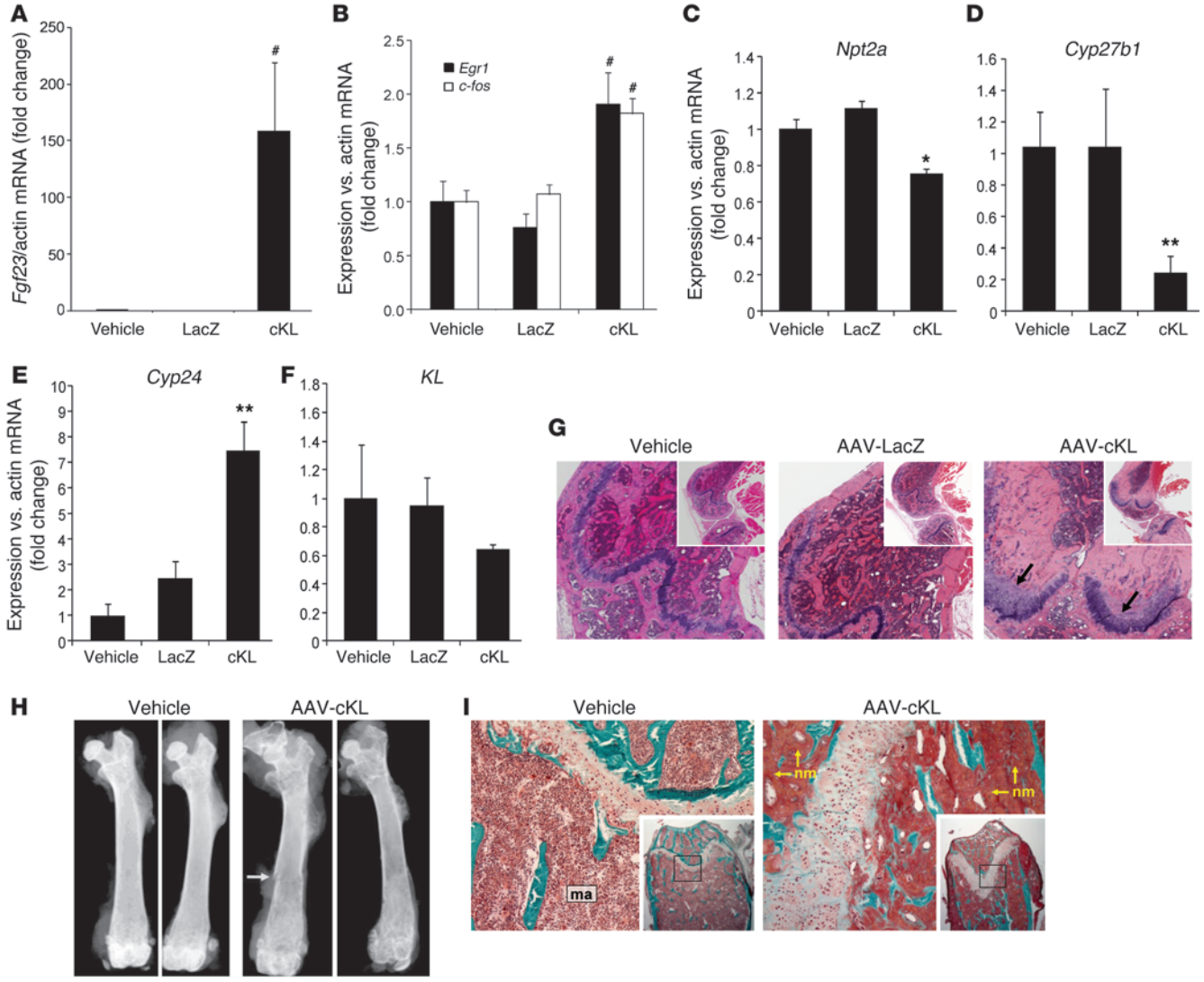

Figure 2

Molecular and skeletal phenotypes with cKL delivery. (**A**) *Fgf23* mRNA was increased in bone harvested from mice 4 weeks following AAV-cKL (1×10^{11} gc per mouse) versus controls. (**B**) *Egr1* and *c-fos* were also elevated in bone following cKL delivery. $^{\#}P < 0.05$ vs. vehicle/LacZ. Reduced renal mRNAs for (**C**) *Npt2a* and (**D**) *Cyp27b1*, with elevated (**E**) *Cyp24*. (**F**) Mice receiving AAV-cKL had no significant change in *KL* (1×10^{11} gc per mouse). $^{*}P < 0.05$, $^{**}P < 0.01$ vs. vehicle/LacZ. (**A**–**F**) Mean ± SEM; $n = 3$–5 per group. (**G**) Compared with controls (left and middle panels), AAV-cKL–treated mice (8 weeks) had widened growth plates at the knee (arrows) (original magnification, ×5; ×2 [inset]). (**H**) Femora from AAV-cKL–treated mice (12 weeks; 1×10^{11} gc per mouse) showed lower radiodensity and had spontaneous fractures (arrow) compared with those from vehicle control mice. (**I**) Goldners'-stained sections revealed an increase in nonmineralized bone (nm) in the high-dose AAV-cKL mice after a 12-week treatment compared with vehicle control. Original magnification, ×10, ×2.5 (inset). ma, marrow.

ure 1A) and hypocalcemia (Figure 1B), with highly elevated bone *Fgf23* mRNA (Figure 2A) and circulating protein (Figure 1D), with metabolic bone disease (Figure 2, G–I). The cKL-treated animals also demonstrated hyperparathyroidism (Figure 1E) similar to that reported in the patient with *KL* translocation. Whether this effect was due to hypocalcemia (Figure 1B) from FGF23-dependent altered 1,25D metabolism or via direct effects of cKL on the parathyroid glands in which αKL is normally expressed remains to be determined. cKL has been implicated as a phosphaturic factor that functions by directly interacting with kidney Npt2a protein to inhibit phosphate reabsorption (5). If the dominant effect of cKL was to induce hypophosphatemia independently of FGF23, following cKL delivery, the predicted endocrine response would be FGF23 suppression. In contrast, the present studies demonstrated that cKL caused robust increases in *Fgf23* mRNA and protein despite the prevailing hypophosphatemia (Figures 1 and 2). Additionally, the renal gene responses for regulators of phosphate and vitamin D metabolism were consistent with elevated FGF23 (Figure 2, C–E) and are reciprocal to those caused by FGF23-independent hypophosphatemia. While potent, cKL is not the sole regulator of FGF23, as αKL-null mice have elevated FGF23, likely driven by 1,25D and/or a yet-identified mechanism for sensing hyperphosphatemia. The AAV-cKL–treated mice had severe osteomalacia (Figure 2), consistent with the prevailing hypophosphate-

Table 1
μCT analysis of skeletal sites in 8-week-old mice

Bone parameter	Vehicle	AAV-LacZ	AAV-cKL (3×10^{10})	AAV-cKL (1×10^{11})
DF total BMD (mg/cm^3)	344.4 ± 5.00	323.9 ± 19.59	227.8 ± 4.76^{A,B}	217.4 ± 35.20^{A,B}
DF total area (cm^2)	0.0338 ± 0.0007	0.0384 ± 0.0048	0.0310 ± 0.002^{A}	0.0311 ± 0.006
DF total BMC (mg)	1.05 ± 0.026	1.09 ± 0.049	0.638 ± 0.053^{A,B}	0.605 ± 0.088^{A,B}
MF total BMD (mg/cm^3)	514.04 ± 6.79	498.6 ± 8.02	344.48 ± 21.11^{A,B}	313.12 ± 29.68^{A,B}
MF total area (cm^2)	0.0170 ± 0.0002	0.0174 ± 0.0003	0.0152 ± 0.0004^{A,B}	0.0160 ± 0.0004^{A,B}
MF total BMC (mg)	0.7887 ± 0.017	0.7831 ± 0.02	0.4724 ± 0.03^{A,B}	0.4539 ± 0.05^{A,B}
LV total BMD (mg/cm^3)	301.76 ± 9.50	367.78 ± 27.98^{A}	227.54 ± 16.83	253.48 ± 21.60
LV total area (cm^2)	0.0531 ± 0.001	0.0472 ± 0.004	0.0412 ± 0.004^{A}	0.0227 ± 0.004^{A,B}
LV total BMC (mg)	1.443 ± 0.06	1.5256 ± 0.08	0.8248 ± 0.07^{A,B}	0.4845 ± 0.07^{A,B}

DF, distal femur; MF, midshaft femur; LV, lumbar vertebra. n = 5 mice per group. $^{A}P < 0.05$ vs. vehicle; $^{B}P < 0.05$ vs. AAV-LacZ.

mia (Figure 1A), as we detected an increase in total trabecular bone driven by an increase in nonmineralized tissue (Supplemental Table 1). The activity of cKL was selective for FGF23 (Figure 3), which supports the concept of cKL potentially regulating FGF23 production through cKL-FGF23-FGFR interactions (Figure 3) in bone, the primary source of this hormone. Consistent with these findings, patients with activating mutations in FGFR1c have elevated plasma FGF23 (12), and reciprocally, suppression of FGFR activity inhibits FGF23 production (13). Whether cKL interacts specifically with FGFR1c in vivo and whether this system could be modulated as a therapeutic target remain to be determined. In conclusion, these studies demonstrate that cKL is an important factor in regulating FGF23 production and significantly modify the current models of phosphate homeostasis, with implications for understanding the control of FGF23 expression during normal and disordered phosphate handling.

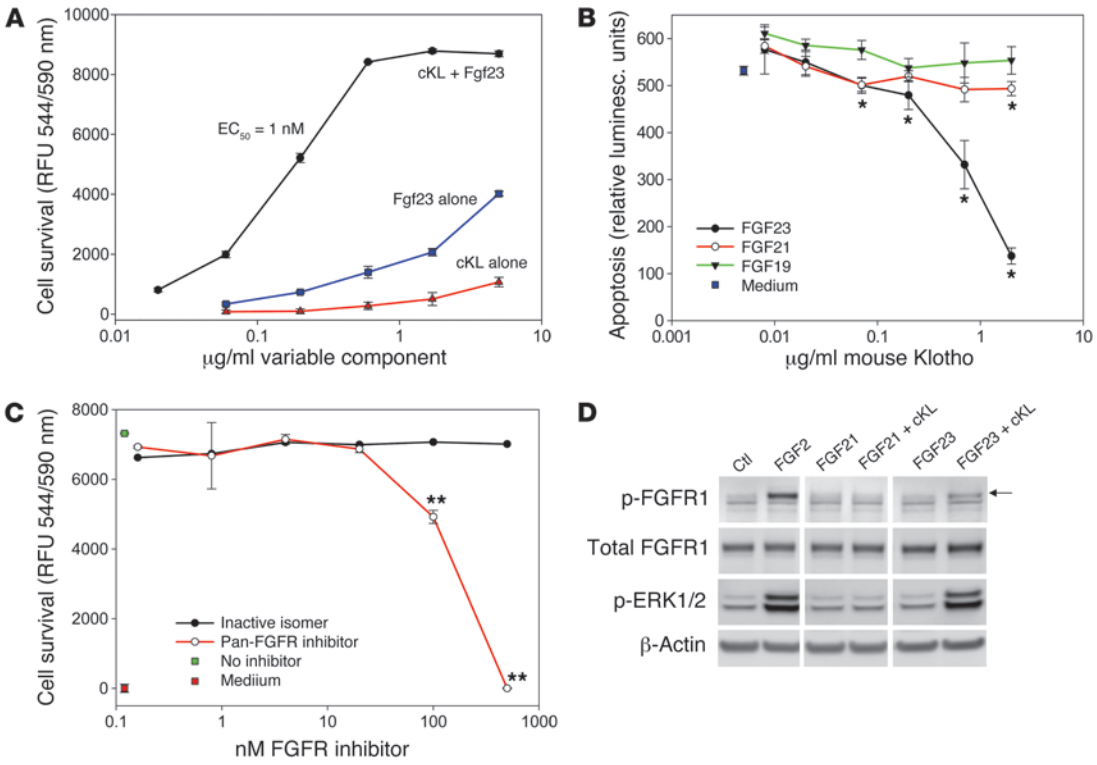

Figure 3
Ligand selectivity of cellular cKL activity. (**A**) NIH3T3 cells were treated with recombinant cKL or FGF23 alone or a combination of the two. FGF23 plus cKL potently increased cell survival (EC_{50}, 1 nM) compared with either alone. (**B**) cKL prevented apoptosis in the presence of FGF23 but not FGF19 or FGF21 (*$P < 0.05$ vs. medium control). (**C**) Pretreatment of NIH3T3 cells with cKL and FGF23 in the presence of a pan-FGFR kinase inhibitor resulted in a significant decrease in cell survival. Cells maintained survival in the presence of the inactive isomer of the inhibitor (also with a reference control with FGF23 plus cKL [No inhibitor]). **$P < 0.01$ vs. inactive isomer. (**A**–**C**) Values are shown as mean ± SEM. (**D**) Immunoblots for p-FGFR1 (arrow) and p-ERK1/2 in L6 cells transfected with FGFR1c, in the presence of the KL-independent ligand FGF2, compared with FGF21 or FGF23 in the presence or absence of cKL. FGF23 elicited FGFR signaling only in the presence of cKL (lanes were from the same gel but were noncontiguous).

Methods

Animal studies

AAV was delivered to 8-week-old C57BL/6 mice via retro-orbital injection, which were then sacrificed by CO_2 inhalation/bilateral pneumothorax or cervical dislocation for biochemical and histological analyses at the indicated times (see the legends for Figures 1 and 2). Mice were retro-orbitally bled at interim time points. Separate cohorts were AAV-treated for 4 weeks for bone and kidney RNA analyses, as this time point coincided with the lowest serum phosphate concentrations.

Recombinant cKL and FGF23 and AAV-cKL production

The cDNA encoding residues 35–983 of the extracellular domain of mouse αKL with a CD33 N-terminal signal sequence, or β-galactosidase gene (*LacZ*) as control, was packaged into a recombinant hybrid adeno-associated viral vector 2/8 (AAV; RegenX Biosciences). In vivo expression was driven by a liver-specific thyroxine-binding globulin promoter. Recombinant cKL and FGF23 protein were produced as previously reported (14) (provided by R. Micanovic, Eli Lilly and Company) or purchased as prepared reagents (R&D Systems).

Cell culture and in vitro functional assays

NIH3T3 cells were cultured according to the distributor's specifications (ATCC). Cell survival was quantified at 72 hours using Resazurin (R&D Systems) according to manufacturer's instructions. To measure apoptosis, cells were treated for 24 hours, and caspase-3/7 activity was quantified using the Caspase-Glo Kit (Promega). Cells were treated with the pan-FGFR inhibitor *LY2874453* (biochemical IC_{50}s for FGFR1 = 0.014 μM; FGFR2 = 0.0032 μM; FGFR3 = 0.0054 μM; and FGFR4 = 0.0495 μM) or its inactive isomer *LY2202696* (provided by G. Zhao, Eli Lilly and Company). L6-hFGFR1c cells (from M. Malabunga, ImClone Systems Inc.) were prepared and cultured as described previously (15). L6-hFGFR1c cells were pretreated with 1 μg/ml mouse αKL (R&D Systems) for 30 minutes and then stimulated with 100 ng/ml human FGF21 or FGF23 (R&D Systems) or 30 ng/ml FGF2 (Life Technologies) for 15 minutes.

Skeletal analyses

Histomorphometry. Bones were preserved in 10% neutral-buffered formalin; bones were embedded in paraffin (decalcified) or methylmethacrylate, sectioned longitudinally, and stained with H&E or Goldners' trichrome. Mineralized bone volume/tissue volume (BV/TV) and nonmineralized BV/TV were assessed in a 2-mm region of the secondary spongiosa of the distal femur on Goldners'-stained methylmethacrylate sections.

CT analyses. Femora and vertebrae were analyzed by quantitative μCT using an LTC-100 CT scanner (Aloka). Scans of the femora were taken at 2 and 10 mm from the end of the growth plate for distal metaphysis and midshaft analyses, respectively. BMC and bone area were calculated using Aloka software (SYS-C320 version 1.5); BMD was calculated as BMC normalized to bone volumetric area.

RNA isolation and qPCR

Femur and kidney RNA were harvested using TRIzol (Life Technologies), and RNA samples were tested with primers specific for mouse *Fgf23*, *Egr1*, *c-fos*, *Cyp27b1*, *Cyp24*, *Npt2a*, and internal control β-actin as previously described (16). The TaqMan One-Step RT-PCR Kit (Life Technologies) was used to perform qPCR, and data were collected using the 7500 Real-Time PCR system and software (Life Technologies) and analyzed using the $2^{-\Delta\Delta CT}$ method.

Immunoblotting

Liver samples were homogenized in lysis buffer (Cell Signaling Technology) on ice using a rotor-stator homogenizer. Immunoblot analysis was performed similar to that previously described (8), with 50 μg lysates per sample. Blots were acid stripped and reprobed with anti-actin-HRP (1:25,000; Sigma-Aldrich). L6-hFGFR1c cell lysates were blotted as described previously (15) and also probed with anti-phospho-ERK1/2 and anti–β-actin (Cell Signaling Technology).

Serum biochemistries

Calcium and Inorganic Phosphorous Reagent Kits (Roche) were used for serum measurements in a Hitachi analyzer (Roche Diagnostics). Serum FGF23 was tested using an "intact" FGF23 ELISA (Kainos Laboratories). Parathyroid hormone (PTH) was measured using a mouse-specific PTH ELISA (Immutopics International), and plasma cKL was quantified using a sandwich ELISA prepared with polyclonal antibodies recognizing the extracellular domain of mouse αKL (antibodies AF1819 and BAF1819; R&D Systems).

Statistics

Statistical analyses of the data were performed by 2-tailed Student's *t* test, and significance for all tests was set at $P < 0.05$.

Study approval

Animal studies were approved by the Indiana University Institutional Animal Care and Use Committee and the internal review board at Eli Lilly and Company and are in accord with NIH guidelines for humane treatment of laboratory animals.

Acknowledgments

The authors acknowledge support from NIH grants DK063934 and AR059278 (to K.E. White). We would like to thank Patrick I. Eacho for early discussions, Keith W. Condon for histology advice, and Armando R. Irizarry and John L. Vahle for histopathology advice.

Received for publication May 29, 2012, and accepted in revised form September 20, 2012.

Address correspondence to: Kenneth E. White, Indiana University School of Medicine, Department of Medical and Molecular Genetics, 975 W. Walnut St., IB130, Indianapolis, Indiana 46202, USA. Phone: 317.278.1775; Fax: 317.274.2293; E-mail: kenewhit@iupui.edu.

1. Urakawa I, et al. Klotho converts canonical FGF receptor into a specific receptor for FGF23. *Nature*. 2006;444(7120):770–774.
2. Kurosu H, et al. Regulation of fibroblast growth factor-23 signaling by klotho. *J Biol Chem*. 2006; 281(10):6120–6123.
3. Matsumura Y, Aizawa H, Shiraki-Iida T, Nagai R, Kuro-o M, Nabeshima Y. Identification of the human klotho gene and its two transcripts encoding membrane and secreted klotho protein. *Biochem Biophys Res Commun*. 1998;242(3):626–630.
4. Imura A, et al. Secreted Klotho protein in sera and CSF: implication for post-translational cleavage in release of Klotho protein from cell membrane. *FEBS Lett*. 2004;565(1–3):143–147.
5. Hu MC, et al. Klotho: a novel phosphaturic substance acting as an autocrine enzyme in the renal proximal tubule. *FASEB J*. 2010;24(9):3438–3450.
6. Brownstein CA, et al. A translocation causing increased alpha-klotho level results in hypophosphatemic rickets and hyperparathyroidism. *Proc Natl Acad Sci U S A*. 2008;105(9):3455–3460.
7. Tenenhouse HS, Econs MJ. Mendelian hypophosphatemias. In: Scriver CR, Beaudet BL, Sly WS, Valle D, eds. *The Metabolic and Molecular Bases of Inherited Disease*. 8th ed. New York, New York, USA: McGraw-Hill Professional; 2001:1–9.
8. Farrow EG, Davis SI, Summers LJ, White KE. Initial FGF23-mediated signaling occurs in the distal convoluted tubule. *J Am Soc Nephrol*. 2009; 20(5):955–960.
9. Farrow EG, Summers LJ, Schiavi SC, McCormick JA, Ellison DH, White KE. Altered renal FGF23-mediated activity involving MAPK and Wnt: effects of the Hyp mutation. *J Endocrinol*. 2010;207(1):67–75.
10. Perwad F, Azam N, Zhang MY, Yamashita T, Tenenhouse HS, Portale AA. Dietary and serum phosphorus regulate fibroblast growth factor 23 expression and 1,25-dihydroxyvitamin D metabolism in mice.

Endocrinology. 2005;146(12):5358–5364.
11. Medici D, et al. FGF-23-Klotho signaling stimulates proliferation and prevents vitamin D-induced apoptosis. *J Cell Biol*. 2008;182(3):459–465.
12. White KE, et al. Mutations that cause osteoglophonic dysplasia define novel roles for FGFR1 in bone elongation. *Am J Hum Genet*. 2005;76(2):361–367.
13. Wohrle S, et al. FGF receptors control vitamin D and phosphate homeostasis by mediating renal FGF-23 signaling and regulating FGF-23 expression in bone. *J Bone Miner Res*. 2011;26(10):2486–2497.
14. Kharitonenkov A, et al. FGF-21/FGF-21 receptor interaction and activation is determined by beta-Klotho. *J Cell Physiol*. 2008;215(1):1–7.
15. Sun HD, et al. Monoclonal antibody antagonists of hypothalamic FGFR1 cause potent but reversible hypophagia and weight loss in rodents and monkeys. *Am J Physiol Endocrinol Metab*. 2007; 292(3):E964–E976.
16. Farrow EG, et al. Iron deficiency drives an autosomal dominant hypophosphatemic rickets (ADHR) phenotype in fibroblast growth factor-23 (Fgf23) knock-in mice. *Proc Natl Acad Sci U S A*. 2011; 108(46):E1146–E1155.